Latin American Journal of Solids and Structures
www.lajss.org

An Enhanced Random Vibration and Fatigue Model for Printed Circuit Boards

Abstract

Aerospace vehicles are mostly exposed to random vibration loads during its operational lifetime. These harsh conditions excites vibration responses in the vehicles printed circuit boards, what can cause failure on mission functionality due to fatigue damage of electronic components. A novel analytical model to evaluate the useful life of embedded electronic components (capacitors, chips, oscillators etc.) mounted on Printed Circuit Boards (PCB) is presented. The fatigue damage predictions are calculated by the relative displacement between the PCB and the component, the lead stiffness, as well the natural vibration modes of the PCB and the component itself. Statistical methods are used for fatigue cycle counting. The model is applied to experimental fatigue tests of PCBs available on literature. The analytical results are of the same magnitude order of the experimental findings.

Keywords

Random vibration, fatigue, PCB.

Bruno de Castro Braz [a, *]
Flávio Luiz de Silva Bussamra [b]

[a] Space System Division, Instituto Nacional de Pesquisas Espaciais, São José dos Campos, Brazil.
Email: bruno.braz@inpe.br
[b] Aerospace Engineering Division, Instituto Tecnológico de Aeronáutica, São José dos Campos, Brazil.
Email: flaviobu@ita.br

* Corresponding author

http://dx.doi.org/10.1590/1679-78253163

Received 13.06.2016
In revised form 10.04.2017
Accepted 05.09.2017
Available online 15.09.2017

1 INTRODUCTION

Aerospace vehicles (airplanes, launcher vehicles and satellites) are exposed to harsh random vibrating environments. These mechanical stresses occur during qualification and acceptance tests, launching and orbit injection (spacecraft) and during continuous flight operations (airplanes). The aerospace vehicles shall be designed to withstand these conditions, providing a safe environment to the onboard equipment. Electronic equipment is constituted mainly of Printed Circuit Boards (PCB) and a support structure, which shall ensure a proper mechanical, thermal and electrical environment to the embedded electronic components (EC), as capacitors, resistors, chips, oscillators etc. The design of aerospace equipment shall be capable to predict the time to failure of the electronic

components. Random vibration is the common environment of aerospace vehicles, then, fatigue calculations are treated statistically.

Wong et al. (2000), Wu (2009) and Grieu et al. (2008) presented stress calculations at PCBs and ECs based on accurate Finite Element Method (FEM) modeling. The methodology consisted of meshing the entire PCB and the electronic component parts, as leads and body. This approach seems to be too time consuming when applied to PCBs with several components. Cifuentes (1994), Yang et al. (2000), Amy et al. (2010, 2006) and Sayles and Stoumbos (2015) proposed simplified FEM models for calculation of PCB's eigenvalues and eigenvectors. The mounted components on the board were modeled by updating the mass and stiffness properties of the PCB.

Experimental vibration tests were presented by Singal et al. (1992), Amy et al. (2010, 2009) and Yang et al. (2002). Veprik and Barbitsky (2000), Veprik (2003) and Esser and Huston (2003) presented experimental data for damped systems. The experimental approach validates only the tested or similar setups, so additional tests are necessary for different configurations.

Silva and Gonçalves (2013) proposed an analytical model for lead stress prediction. The leads were modeled as beams, the EC as a 6-degree-of-freedom rigid bodies and the PCB as a simply supported plate. These authors did not apply a fatigue model for component life evaluation. Steinberg (2000) proposed a semi-analytical method for estimating the useful life of electronic components mounted on PCBs under random vibrations. The PCB was modeled as a beam. The beam displacements were taken into account, but the rotations not. The fatigue damage prediction was performed for an electronic component (EC) in the center of the board, and the results were approximated elsewhere. Steinberg's method is one of the methods most used in aerospace industry.

The objective of this work is to present a novel accurate analytical model with low computational cost for fatigue life prediction of electronic components mounted on PCBs, which typically fails at the leads. The loads at the leads are calculated by the relative displacements and rotations between the PCB and the EC when the system is excited. The PCB is modeled as a thin plate, considering a uniform smearing of electrical component masses. The EC is modeled as: a) a rigid body and b) a system of two perpendicular beams (3-degree-of-freedom system). The fatigue life is evaluated by Dirlik (1985) statistical fatigue damage model.

The present work enhances the well-known semi-analytical method developed by Steinberg (2000) by proposing a plate model (instead of a beam) to the PCB, adding the contributions of the PCB rotations, the EC body flexibility and the EC first natural frequency. A similar model seems not to be available in the literature. Also, the present work adopt the Dirlik's random fatigue damage counting method (instead of the 3-band technique), one of the methods most used in industry for fatigue calculations. Steinberg's method compensates the lack of these features by the use of the experimental constant C_{st} , defined in his book for each type of electronic component. The Steinberg's method is given by

$$N = 20 \cdot 10^6 \left\{ \left(\frac{0.00022 \cdot 25.4^{1.5} B_{PCB}}{C_{st} t_{PCB} r \sqrt{L}} \right) \cdot \frac{1}{Z_{\max\_rms}} \right\}^{b_b} , \tag{1}$$

where, N is the cycles to failure, B_{PCB} is the PCB length, L is the EC length parallel to B_{PCB} , r is a factor given by a sine function to account the EC position on the PCB (r = 1 in the PCB's center, r

< 1 in the other regions), C_{st} is a constant for different types of ECs, t_{PCB} is the PCB thickness and Z_{max_rms} is the root mean square of the PCB maximum displacement, all given in millimeters.

2 ELECTRONIC COMPONENT LEADS FATIGUE

Electronic components can be simply approximated by three different parts. The main part is the component body, usually covered by a case made of plastic or ceramic. The leads connect the component to the PCB circuitry. The third part is the solder joints, which attach the leads to the board. The typical failure of electronic components under vibration is the fatigue of leads and/or solder joints due to the relative displacements between the component and the PCB.

The lead is assumed as a beam with bending, axial and torsional stiffness. The lead geometry is modeled with the polygonal form exhibited in Fig. 1. For simpler cases some quotas can be set to zero.

The lead fatigue life model is presented below. Section 2.1 describes the lead stiffness calculations, followed by the lead stretch model definition on Section 2.2. The formulation is extended to account for the component body flexibility (Sections 2.3 and 2.4) and PCB bending rotations (Sections 2.5 and 2.6). At last, the stresses (Section 2.7) and the fatigue damage (Section 2.8) complete the model.

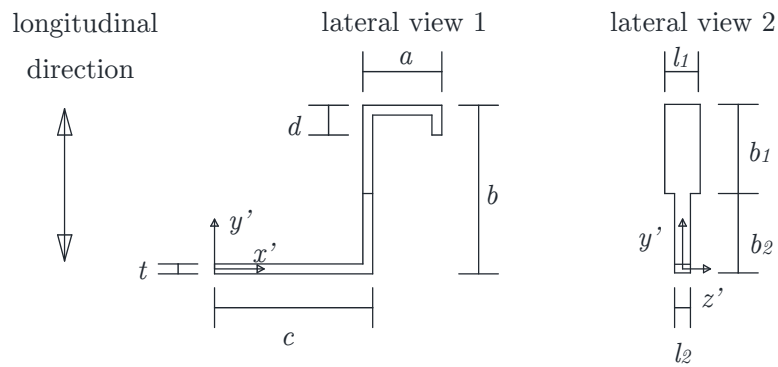

Figure 1: Simplified (polygonal) lead geometry.

2.1 Lead Stiffness

Figure 2a shows the free-body diagram of a lead when the component moves perpendicular to the PCB plane (lead longitudinal direction). The model considers that the leads are clamped on the component body (extremity 1), which is so far adopted rigid, and the deformed PCB applies an external force P at extremity 2 (solder joint). Figures 2b and 2c present the free-body diagrams when the PCB curvature introduces bending and torsional moments, M and T, respectively, at point 2.

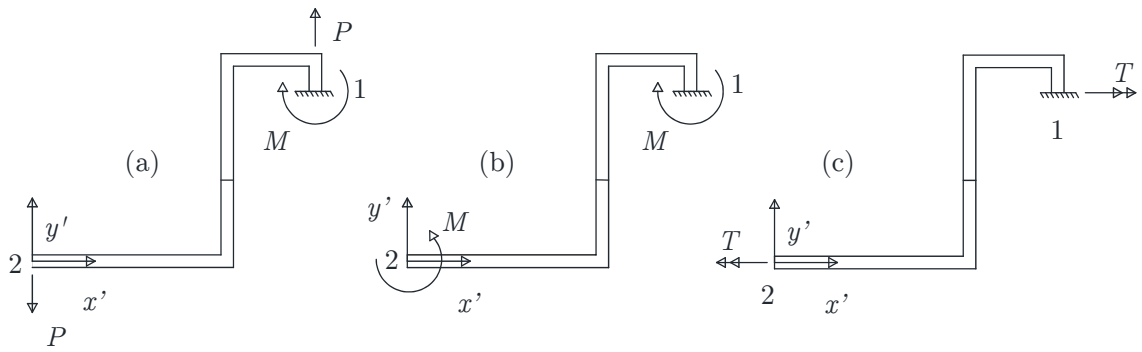

Figure 2: Lead free-body diagrams: (a) concentrated lead P; (b) bending moment M; (c) torsional moment T.

Based on Euler-Bernoulli beam theory, the lead stiffness in the lead longitudinal direction due to a force P is given by

$$k_l = \left\{ \left(\frac{c^3}{3EI_{z'2}} + \frac{b_2 c^2}{EI_{z'2}} + \frac{b_1 c^2}{EI_{z'1}} + \frac{\left(a^3 + 3a^2 c + 3ac^2\right)}{3EI_{z'1}} - \frac{\left(a+c\right)^2 d}{EI_{z'1}} \right) + \left(\frac{b_1 + d}{EA_1} + \frac{b_2}{EA_2} \right) \right\}^{-1}, \tag{2}$$

where E is the elasticity modulus of the lead, $I_{z'i}$ and A_i are respectively the moment of inertia parallel to z' axis taken at the section geometric center and the cross section area of the part i, i =1,2 (b_1, b_2), as depicted in Fig. 1 (lateral view 2).

Similarly, the bending and torsional stiffness are given by, respectively,

$$k_b = \left(\frac{c}{EI_{z'2}} + \frac{b_2}{EI_{z'2}} + \frac{b_1}{EI_{z'1}} + \frac{a}{EI_{z'1}} - \frac{d}{EI_{z'1}} \right)^{-1}, \tag{3}$$

$$k_t = \left(\frac{c}{GJ_2} + \frac{b_2}{EI_{x'2}} + \frac{b_1}{EI_{x'1}} + \frac{a}{GJ_1} - \frac{d}{EI_{x'1}} \right)^{-1}, \tag{4}$$

where G is the shear modulus of elasticity, J_i and $I_{x'i}$ are respectively the polar moment of inertia and the moment of inertia parallel to x' axis taken at the section geometric center of the part i, i =1,2 (b_1, b_2).

2.2 Lead Stretch

The lead stretches are due to the PCB displacements and the EC acceleration. The PCB is modeled as a simply supported rectangular plate of dimensions $\bar{a} \times \bar{b}$. The x- y coordinate system origin is located on the PCB left lower corner, and the x_c- y_c EC local coordinate system is located on component center, as depicted in Fig. 3.

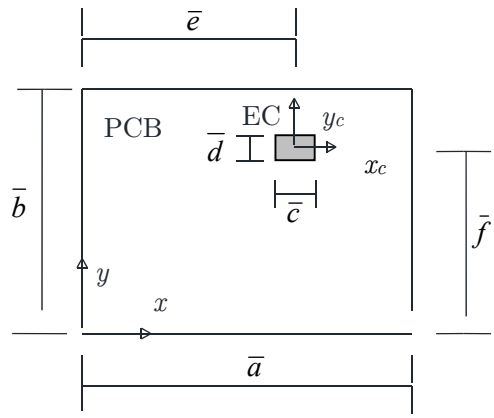

Figure 3: PCB with an electronic component (EC).

The leads local coordinate system x'- y' is perpendicular to the plane x- y of the PCB: x' lays on the x- y plane and y' is perpendicular to this plane. The W_{mn} natural frequencies of the PCB and its Z_{mn} displacements are given by (Blevins 2001)

$$W_{mn} = \pi^2 \left[\left(\frac{m}{\bar{a}} \right)^2 + \left(\frac{n}{\bar{b}} \right)^2 \right] \sqrt{\frac{E_{PCB} t_{PCB}^3}{12 \rho_{PCB} \left(1 - \upsilon_{PCB}^2 \right)}}, \tag{5}$$

$$Z_{mn}\left(x, y, W\right) = \frac{2 B_{mn}\left(W\right)}{\sqrt{\rho \bar{a} \bar{b}}} \sin\left(\frac{m \pi x}{\bar{a}} \right) \sin\left(\frac{n \pi y}{\bar{b}} \right), \tag{6}$$

where m and n are the number of half waves in x and y directions, respectively. E_{PCB}, t_{PCB}, ρ_{PCB} and υ_{PCB} are the PCB elasticity modulus, thickness, density and Poisson's ratio. The PCB density ρ_{PCB} is the ratio between the total mass of the system (PCB plus ECs) and the volume of the PCB. $B_{mn}(W)$ determines the vibration magnitude. For a uniform acceleration distribution α over the PCB, B_{mn} is given by

$$B_{mn}\left(W\right) = G_{mn}\left(W\right) \alpha\left(W\right), \tag{7}$$

where

$$G_{mn}\left(W\right) = \frac{-\frac{2\sqrt{\rho a b}}{\pi^2 m n} \left(1 - \cos\left(\pi m\right)\right)\left(1 - \cos\left(\pi n\right)\right)}{W_{mn}^2 - W^2 + 2 i \xi W_{mn} W}. \tag{8}$$

So far, it is assumed that the PCB and the leads are both flexible, all the displacements are small ($sen\theta \tilde{} \theta$), and the electronic component body is a rigid plate. Then the transverse (lead longitudinal) displacements can be written as

$$Z_{c,mn}\left(x,y\right)=Z_0+\left(x-\overline{e}\right)\theta_c+\left(y-\overline{f}\right)\varphi_c \quad , \quad \overline{e}-\frac{\overline{c}}{2}\le x\le\overline{e}+\frac{\overline{c}}{2} \quad , \quad \overline{f}-\frac{\overline{d}}{2}\le y\le\overline{f}+\frac{\overline{d}}{2} \tag{9}$$

where Z_0 stands for displacement in z direction at the center of the EC ($x=\overline{e}$, $y=\overline{f}$) and θ_c (or ϕ_c) is the rotation around x (or y) axis, as displayed in Fig. 4. These values are determined considering a uniform distribution of springs connecting the component to the board and the equilibrium equations (details at Appendix A).

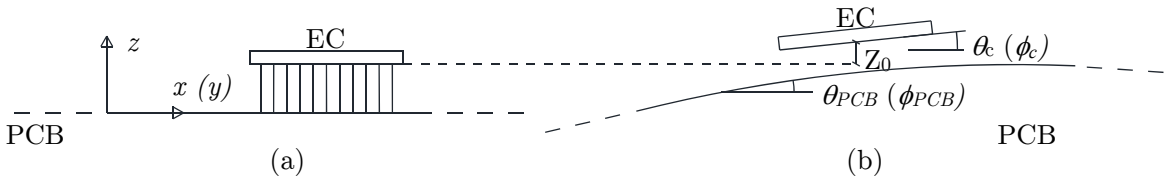

Figure 4: Kinematics of the PCB and EC: (a) underformed position; (b) displacement and rotations.

Now, it is possible to determine the $\delta_{cg,mn}$ lead stretch in the position (x,y) and in the W frequency due to the PCB vibration as

$$\delta_{cg,mn}\left(x,y,W\right)=Z_{c,mn}-Z_{mn}=\delta_{mn}\left(x,y,W\right)B_{mn}, \tag{10}$$

where δ_{mn} is a transfer function from B_{mn} to δ_{cg_mn} .

In addition to the stretches due to the PCB displacement, the acceleration itself induces a mass/spring/damper behavior on the component, modeled as a 1-degree-of-freedom system with total stiffness calculated as the sum of all n leads k_l (Eq. 2). The component natural frequency, vibration transfer function and stretch due to the acceleration are given respectively by

$$W_{c,long}=\sqrt{\frac{nk_l}{m_c}}, \tag{11}$$

$$G_{c,long}\left(W\right)=\frac{-1}{W_{c,long}^2-W^2+2i\xi_{c,long}W_{c,long}W}, \tag{12}$$

$$\delta_{ca,mn}\left(x,y,W\right)=\left[Z_{mn}\left(x,y\right)G_{mn}\left(W\right)\left(-W^2\right)+1\right]G_{c,long}\left(W\right)\alpha\left(W\right), \tag{13}$$

where m_c is the total mass of the electronic component (EC), $\xi_{c,long}$ is the lead damper coefficient, adopted as 0.05 (as usual for some metal alloys) and i is the complex number.

2.3 Component Body Flexibility to Displacements

In the previous Section, the geometric stretch $\delta_{cg,mn}$ and the acceleration stretch $\delta_{ca,mn}$ are calculated assuming the component to be a rigid body. However, the component body is flexible and absorbs part of the strain, what relieves the stresses on the leads. The component flexibility calcula-

tion is not a trivial task, because the lead itself is a flexible structure and the loads are dependent on the component position and on the PCB vibration mode. The EC is supposed to be a rectangle of side lengths $\overline{c} \times \overline{d}$. Each lead, located on the EC boundary at distances l_x and l_y from the EC center, applies a concentrated load P, as shown in Fig. 5. The EC is modeled as a sum of two distinct beams clamped in the component center, where R_x and R_y are the fractions of the load applied on each direction:

$$R_x = \frac{l_x}{l_x + l_y} \quad , \quad R_y = \frac{l_y}{l_x + l_y}. \tag{14}$$

Therefore, the total component body displacement (δ_c) at the lead is the sum of the displacements due to the $R_x P$ force ($\delta_{c,x}$), and due to the $R_y P$ force ($\delta_{c,y}$), say

$$\delta_c = \delta_{c,x} + \delta_{c,y}, \tag{15a}$$

$$\delta_{c,x} = \frac{\overline{c}^3 R_x P}{24 E I_{x,c}} \quad , \quad \delta_{c,y} = \frac{\overline{d}^3 R_y P}{24 E I_{y,c}}, \tag{15b}$$

where E is the elasticity modulus, $I_{x,c}$ and $I_{y,c}$ are the inertia moment around x_c and y_c axes (Fig. 5) and t_c the component body thickness. The EC inertia moments are calculated considering an internal void of $t_c/2$:

$$I_{x,c} = \frac{\overline{d}\left[t_c^{\,3} - \left(t_c / 2\right)^3\right]}{12} \quad , \quad I_{y,c} = \frac{\overline{c}\left[t_c^{\,3} - \left(t_c / 2\right)^3\right]}{12}. \tag{16}$$

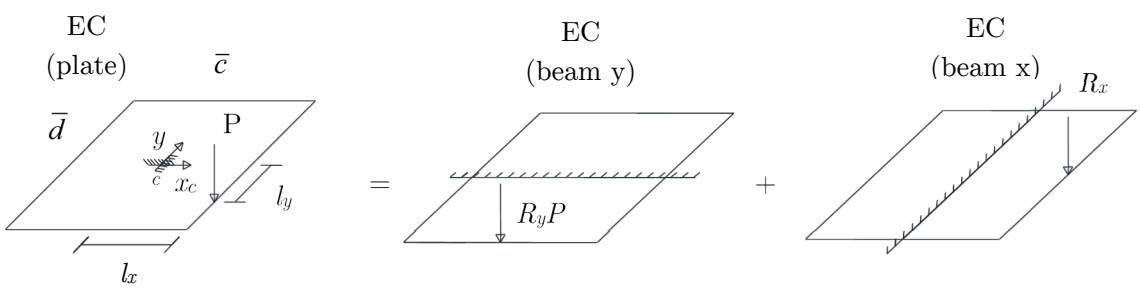

Figure 5: Double-beam model for EC.

The force applied on the component body equals to the force applied on the leads, and the total stretch is the sum of the component stretch and the lead stretch ($\delta_{lead,x}$, $\delta_{lead,y}$). For equilibrium of EC

$$R_x P = \frac{24 E I_{x,c}}{\overline{c}^3} \delta_{c,x} = k_l n_x \delta_{lead,x}\,, \tag{17}$$

then

$$\delta_{c,x} = \frac{\overline{c}^3 k_l n_x}{24EI_{x,c}} \delta_{lead,x} \quad , \quad \delta_{c,y} = \frac{\overline{d}^3 k_l n_y}{24EI_{y,c}} \delta_{lead,y} , \tag{18}$$

where n_x and n_y are the number of leads on each side of length $\overline{d}$ and $\overline{c}$, respectively. Thus, the total stretch δ can be calculated as the sum of leads and component body stretches

$$\delta = \left(\frac{\overline{c}^3 k_l n_x}{24EI_{x,c}} + 1 \right) \delta_{lead,x} + \left(\frac{\overline{d}^3 k_l n_y}{24EI_{y,c}} + 1 \right) \delta_{lead,y} . \tag{19}$$

Assuming a linear relation between lead stretches $\delta_{lead,x}$ and $\delta_{lead,y}$, with $R_x + R_y = 1$, the total stretch and consequently the fat_c lead stretch reduction factor can be written as

$$\delta_{lead,x} = R_x \delta_{lead} \quad , \quad \delta_{lead,y} = R_y \delta_{lead} , \tag{20}$$

$$\delta = fat_c \left(x, y \right)^{-1} \delta_{lead} , \tag{21}$$

where

$$fat_c \left(x, y \right) = \left(\frac{R_x \overline{c}^3 k_l n_x}{24EI_{x,c}} + \frac{R_y \overline{d}^3 k_l n_y}{24EI_{y,c}} + 1 \right)^{-1} . \tag{22}$$

2.4 Lead Total Stretch

The $\delta_{c,long}$ total lead stretch can be calculated for all PCB vibration modes from Eqs. 10, 13 and 22

$$\begin{aligned} \delta_{c,long} = \sum_{m,n=1,1}^{m,n=\varphi,\varphi} \left[\delta_{cg,mn} + \delta_{ca,mn} \right] fat_c = \sum_{m,n=1,1}^{m,n=\varphi,\varphi} \Big\{ & \delta_{mn} \left(x, y, W \right) G_{mn} \left(W \right) \\ & + \left[Z_{mn} \left(x, y \right) G_{mn} \left(W \right) \left(-W^2 \right) + 1/\varphi^2 \right] G_{c,long} \left(W \right) \Big\} fat_c \left(x, y \right) \alpha \left(W \right). \end{aligned} \tag{23}$$

Note that the term 1 is divided by φ^2 in order to not account φ^2 times the α input acceleration.

2.5 Lead Rotation

The lead rotations are caused by the PCB bending curvature during the vibrations (θ_{PCB} or ϕ_{PCB}) minus the component body rotation (θ_c or ϕ_c) and minus the rotation due to the lead longitudinal stretch (θ_2 - see Appendix A). The PCB rotations, which induce torsional and bending moments, are given by the derivative of Eq. 6 by x and y. The rotations necessary to describe the problem are depicted in Fig. 4 and summarized at Appendix A.

2.6 Component Body Flexibility to Rotations

The component body flexibility to rotations and moments shall also be applied to the model. The flexibility factor due to rotations differs from the flexibility factor due to forces by the difference in beam stiffness for these two distinct types of loads. The cantilever beam stiffness to moments is

$$k_{beam,moment} = \frac{EI}{L}, \tag{24}$$

then, the flexibility factors for bending and torsional moments assume a slightly different format

$$fat_{cm1}\left(x,y\right) = \left(\frac{R_x\left(x,y\right)\overline{c}k_b n_x}{2EI_{x,c}} + \frac{R_y\left(x,y\right)\overline{d}k_b n_y}{2EI_{y,c}} + 1 \right)^{-1} fat_c\left(x,y\right), \tag{25}$$

$$fat_{cm2}\left(x,y\right) = \left(\frac{R_x\left(x,y\right)\overline{c}k_t n_x}{2EI_{x,c}} + \frac{R_y\left(x,y\right)\overline{d}k_t n_y}{2EI_{y,c}} + 1 \right)^{-1} fat_c\left(x,y\right), \tag{26}$$

where fat_c is the flexibility reduction factor for force (Eq. 22), fat_{cm1} is the flexibility reduction factor for lead bending rotations (Fig. 2b), and fat_{cm2} is the flexibility reduction factor for lead torsional rotations (Fig. 2c). In the same way fat_c multiplies the lead total stretch (Eq. 23), fat_{cm1} multiplies the lead total bending rotation around y and x, and fat_{cm2} multiplies the lead total torsional rotation around y and x, as presented on Appendix A (Eqs A.8-11). The inclusion of fat_c in Eqs. 25 and 26 is a simplified way to account for component body additional rotation due to the longitudinal stretches.

2.7 Lead Stress

The stretches and rotations found on the previous Sections are now used to evaluate the lead stress. The von Mises stress is directly proportional to the input acceleration

$$\sigma_{VM}\left(x,y,W\right) = G_{VM}\left(x,y,W\right)\alpha\left(W\right), \tag{27}$$

where G_{VM} is the transfer function from input acceleration α to the von Mises stress σ_{VM}. For random vibrations, the variables are described in Power Spectral Density (PSD) (Lalanne 2002), resulting in

$$\sigma_{VM,PSD}\left(x,y,W\right) = \left|G_{VM}\left(x,y,W\right)\right|^2 \alpha_{PSD}\left(W\right). \tag{28}$$

2.8 Fatigue Damage

The fatigue damage model used on this work is the well-known Miner's rule (Lalanne 2002), where the fatigue damage D is calculated as the relation between the number n_i of performed cycles in a prescribed stress, to the number N_i of cycles necessary to produce a failure in the same stress level, as described in Eq. 29. The failure occurs when $n_i = N_i$.

$$D = \frac{n_i}{N_i}. \tag{29}$$

The fatigue damage in random vibrations, once obtained the stress response in PSD (Eq. 28), is calculated in this work by Dirlik's method (Dirlik 1985), one of the most used in industry and literature. The damage, evaluated with a probability distribution function developed statistically through the use of several random signals and with the Rainflow cycle counting method (ASTM 2011), is calculated as

$$D = n_p^+ T \frac{\left(\sigma_{VM,rms}\right)^{b_b}}{C_b}\left[G_1 Q^{b_b}\Gamma\left(1+b\right) + \left(\sqrt{2}\right)^{b_b}\Gamma\left(1+\frac{b_b}{2}\right)\left(G_2\left|R\right|^{b_b} + G_3\right)\right], \tag{30}$$

where T is the time, $\sigma_{VM,rms}$ is the root mean square of the von Mises stress, Γ is the Gamma function, b_b and C_b are the S-N variables given by Basquin relation ($N\sigma^{b_b} = C_b$), and G_1, G_2, G_3, R and Q are variables defined on Appendix B.

All stresses are directly proportional to the input accelerations. It is possible to affirm that for each PCB vibration mode, the relations between shear and normal stresses are constant. When describing the stresses in PSD, these relations are always constant (in statistical sense) for each frequency band, apart the PCB vibration modes, because all vibration modes are summed (Eq. 23). Finally, as the root mean square of the power spectral densities represents a statistical average of the stresses, it is possible to assume that the relations between shear and normal stresses are in average constant. Therefore, the von Mises root mean square (rms) stress can be used to approximate the fatigue damage calculations in random vibrations, as presented on Eq. 30.

3 RESULTS

The present model is applied to PCB's experimental fatigue tests available on the literature. The results are also compared to Steinberg's method predictions. The experimental results findings discussed in this Section include most of the types of leads, assemblies and solder joints. All materials, dimensions and properties used for each case are presented on Appendix C.

In each system, the model is applied with four distinct configurations in order to clarify the fatigue damage contributors:

1) Complete / 9 modes: the PCB is modeled as a plate with 9 natural vibration modes, and the ECs as double beams with 1 natural mode;
2) Acceleration off: the PCB is modeled as a plate with 9 modes, and the ECs as double beams without the contribution of its natural frequency, expressed by $\delta_{ca,mn}$ (Eq. 13);
3) Moment off: the PCB is modeled as a plate with 9 natural modes, and the ECs as double beams with 1 natural mode and not accounting the influence of PCB curvature;
4) Complete / 1 mode: the PCB is modeled as a plate with only 1 natural mode, and the ECs as double beams with 1 natural mode.

3.1 Plastic Leaded Chip Carrier (PLCC) and Leadless Ceramic Chip Carrier (LCCC)

Liguore and Followell (1995) performed random vibration tests in 8 PCBs with 9 electronic components, 3 of the type PLCC with 68 J-leads and the others of the type LCCC with 32, 68 and 84 pins, as described in Fig. 6. The epoxy fiberglass PCBs (E-Glass) with $152.4 \times 152.4 \times 1.45$ mm^3 were mounted in a shaker with the side close to the components U1, U2 and U3 free. As the analytical model uses a 4-side simply supported plate, the PCB was mirrored about the free edge. The PCBs were vibrated in a band frequency of 50 Hz around the first natural frequency of the board with a constant PSD. The applied levels and PCB's amplifications varied in order to produce results between 30 to 80 G_{rms}.

In the present model, the PLCC leads of copper are modeled with the following geometric parameters: $a = 0.08$ mm, $b_1 = 1.02$ mm, $b_2 = 1.02$ mm, $t = 0.25$ mm, $l_1 = 0.735$ mm and $l_2 = 0.43$ mm. The leads made of Pb solder (LCCC) have more or less conical shape and the rupture often appears in the middle of the cone. Thus the LCCC lead is modeled with the $b_1 = b_2 = 0.85/2$ mm parts and with a constant diameter given by the average ($l_1 = l_2 = 1.27$ mm).

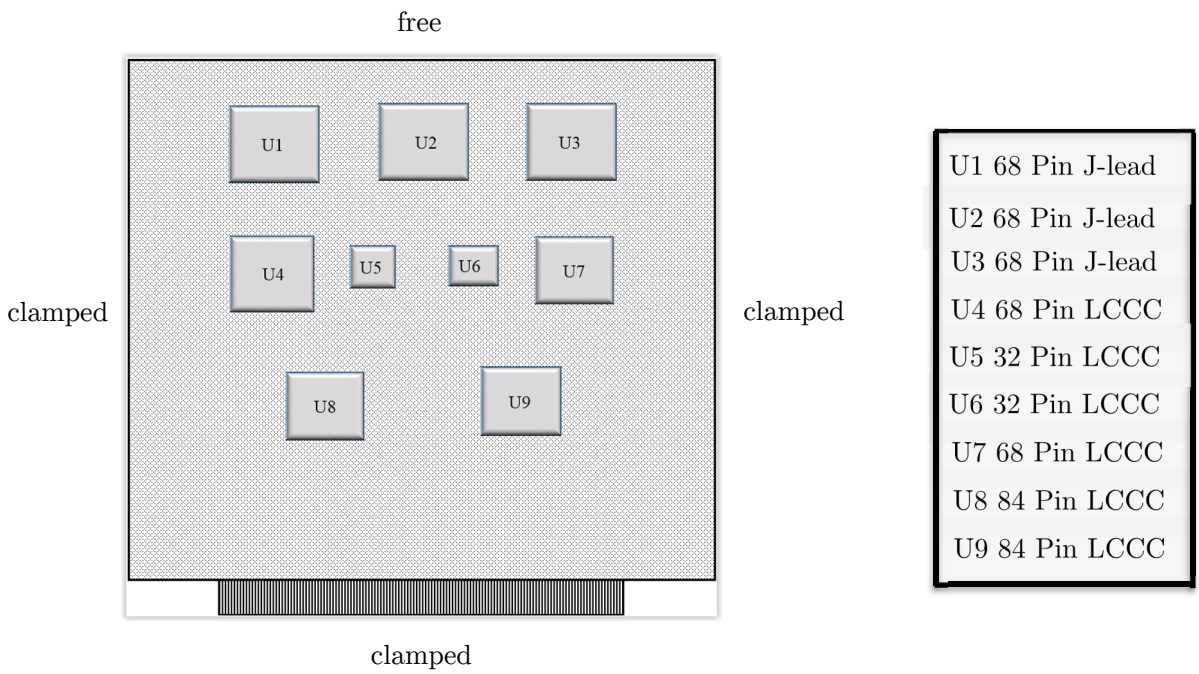

Figure 6: Test setup – PLCC and LCCC (Liguore and Followell 1995).

The results of the present model are exposed in Tables 1 to 5 and compared with experimental results from Liguore and Followell (1995) and semi-analytical beam model from Steinberg (2000). Liguore and Followell (1995) presented their results only for component type. No information about component position was given. So, the results of components U1, U2 and U3 are analyzed altogether. All the present model results are of the same magnitude order of the experimental ones.

The influences of acceleration stretch are lower than 11% in the fatigue life, explained by the ECs calculated natural frequencies 200 times higher than the maximum vibration frequency of 175 Hz. The component with the lower calculated natural frequency is the 68 J-lead (U1, U2 and U3) with 31123 Hz. Also, as the geometrical stretch (Eq. 10) is the main damage contributor for this case, the regions in the diagonal of the board have lower fatigue lives.

The PLCCs have longer fatigue lives than the LCCCs due to the difference in stiffness. Both components have close fat_c factors (Eq. 22). However the LCCC components have ceramic bodies and short leads made of solder, which are stiffer and produce more stresses.

Steinberg's results for all EC but U2 are of the same magnitude order of experimental results since the geometrical stretch is the most damaging contributor in these components. However, it is conservative for the EC in the PCB center region (U2).

Model	U1 and U3 components	U2 component	Fail Point (Fig. 1)
Complete / 9 modes	4.79×10^6	14.73×10^6	a
Acceleration off	5.14×10^6	16.47×10^6	a
Moment off	5.22×10^6	16.00×10^6	a
Complete / 1 mode	4.78×10^6	14.73×10^6	a
Steinberg (2000)	1.96×10^6	0.21×10^6	not available
Liguore and Followell (1995)	1×10^6 to 9×10^6		not available

Table 1: Cycles to failure for PLCC with 30.6 G_{rms}, 68 J-Lead.

Model	U1 and U3 components	U2 component	Fail Point (Fig. 1)
Complete / 9 modes	0.86×10^4	2.65×10^4	a
Acceleration off	0.92×10^4	2.96×10^4	a
Moment off	0.94×10^4	2.87×10^4	a
Complete / 1 mode	0.86×10^4	2.65×10^4	a
Steinberg (2000)	0.37×10^4	0.038×10^4	not available
Liguore and Followell (1995)	2×10^4 to 10×10^4		not available

Table 2: Cycles to failure for PLCC with 80.7 G_{rms}, 68 J-Lead.

Model	U5 and U6 components	Fail Point (Fig. 1)
Complete / 9 modes	5.19×10^5	solder
Acceleration off	5.44×10^5	solder
Moment off	11.52×10^5	solder
Complete / 1 mode	5.19×10^5	solder
Steinberg (2000)	0.90×10^5	not available
Liguore and Followell (1995)	10×10^5 to 40×10^5	solder

Table 3: Cycles to failure for LCCC with 30.6 G_{rms}, 32 pins.

Model	U4 and U7 components	Fail Point (Fig. 1)
Complete / 9 modes	1.87×10^5	solder
Acceleration off	1.90×10^5	solder
Moment off	2.95×10^5	solder
Complete / 1 mode	1.87×10^5	solder
Steinberg (2000)	1.17×10^5	not available
Liguore and Followell (1995)	2×10^5 to 20×10^5	solder

Table 4: Cycles to failure for LCCC with 30.6 G_{rms}, 68 pins.

Model	U8 and U9 components	Fail Point (Fig. 1)
Complete / 9 modes	5.94×10^5	solder
Acceleration off	6.00×10^5	solder
Moment off	8.52×10^5	solder
Complete / 1 mode	5.95×10^5	solder
Steinberg (2000)	0.63×10^5	not available
Liguore and Followell (1995)	2.0×10^5 to 10×10^5	solder

Table 5: Cycles to failure for LCCC with 30.6 G_{rms}, 84 pins.

3.2 Plastic Ball Grid Array (PBGA)

The Plastic Ball Grid Array (PBGA) components are constituted by plastic body and spherical leads of solder. YU et al (2011) presented random vibration results for PBGA with SAC 305 and SAC 405 Pb free solder joints (lead). The tests were performed in FR4 PCBs of dimensions 100 × 50 × 0.6 mm^3 attached to the shaker through 6 screws, as described in Fig. 7. Two tests were performed for each solder configuration, one with 0.15 g^2Hz^{-1}, another with 0.25 g^2Hz^{-1} (PSD), both in 40 to 1000 Hz frequency range.

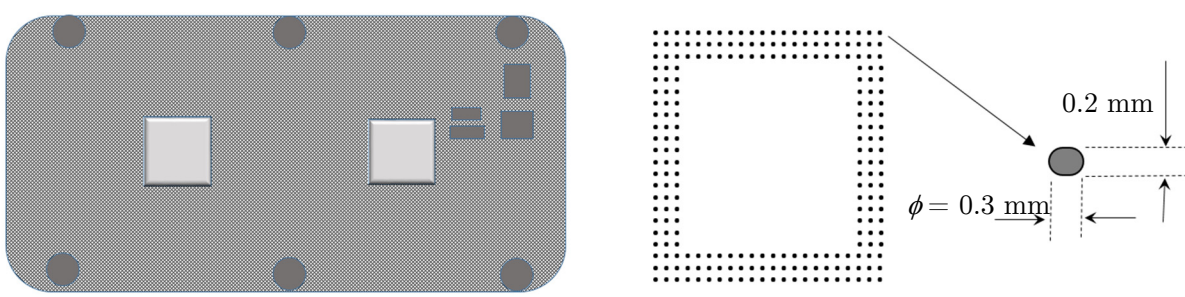

Figure 7: Test setup – PBGA (Yu et al. 2011).

The present model results are obtained by assuming the leads as a cylinder of 2 parts, b_1 and b_2. The first part has the average diameter of l_1 = 0.266 mm and the total length of the solder

joint/lead $b_1 = 0.2$ mm. The second part has a negligible length $b_2 = 0$ and diameter of $l_2 = 0.22$ mm (the smallest diameter of the solder ball), used for stress calculations.

The results are exposed in Tables 6 to 9. As expected from solder leads, the high stiffness of the connection makes the geometric stretch (Eq. 10) the main contributor to the fatigue damage. The components calculated natural frequency is 606320 Hz, which is far beyond the tested frequency band. Therefore, the acceleration stretch contribution was minimized. It is also possible to observe the good adherence of the present predictions.

In this case, Steinberg's method presents results in conformance due to the high contribution of the geometrical stretch, the only structural feature modeled by Steinberg.

Model	$x=\overline{a}$ /4; $y=\overline{b}$ /2 (Fig. 3)	Fail Point (Fig. 1)
Complete / 9 modes	1.27×10^2	solder
Acceleration off	1.33×10^2	solder
Moment off	1.71×10^2	solder
Complete / 1 mode	1.35×10^2	solder
Steinberg (2000)	0.15×10^2	not available
YU et al (2011)	0.1×10^2 to 2.20×10^2 average: 1.13×10^2	solder

Table 6: Minutes to failure for PBGA SAC 305 with 0.25 g^2Hz^{-1}.

Model	$x=\overline{a}$ /4; $y=\overline{b}$ /2 (Fig. 3)	Fail Point (Fig. 1)
Complete / 9 modes	7.61×10^2	solder
Acceleration off	7.99×10^2	solder
Moment off	10.24×10^2	solder
Complete / 1 mode	8.08×10^2	solder
Steinberg (2000)	0.92×10^2	not available
YU et al (2011)	1.0×10^2 to 4.0×10^2 average: 3.95×10^2	solder

Table 7: Minutes to failure for PBGA SAC 305 with 0.15 g^2Hz^{-1}.

Model	$x=\overline{a}$ /4; $y=\overline{b}$ /2 (Fig. 3)	Fail Point (Fig. 1)
Complete / 9 modes	1.41×10^2	solder
Acceleration off	1.46×10^2	solder
Moment off	1.72×10^2	solder
Complete / 1 mode	1.48×10^2	solder
Steinberg (2000)	0.62×10^2	not available
YU et al (2011)	average: 1.02×10^2	solder

Table 8: Minutes to failure for PBGA SAC 405 with 0.25 g^2Hz^{-1}.

Model	$x=\bar{a}/4$; $y=\bar{b}/2$ (Fig. 3)	Fail Point (Fig. 1)
Complete / 9 modes	4.77×10^2	solder
Acceleration off	4.93×10^2	solder
Moment off	5.80×10^2	solder
Complete / 1 mode	4.99×10^2	solder
Steinberg (2000)	2.09×10^2	not available
YU et al (2011)	average: 2.82×10^2	solder

Table 9: Minutes to failure for PBGA SAC 405 with 0.15 g^2Hz^{-1}.

3.3 Plastic Dual in-line Package (PDIP) and Tantalum Capacitor

The Plastic Dual in-line Package (PDIP) components are composed of a plastic body with 14 leads mounted on 2 parallel sides. The Tantalum capacitors are cylindrical components with 2 leads. Genç (2006) tested 6 PCBs, 3 fully populated with 24 PDIPs (Fig. 8a) and other 3 fully populated with 30 capacitors (Fig. 8a). Both components were mounted on the boards by through hole solder joints. All the PCBs are of 233 × 15 × 1 mm^3 dimensions, attached to the shaker as shown on Fig. 8.

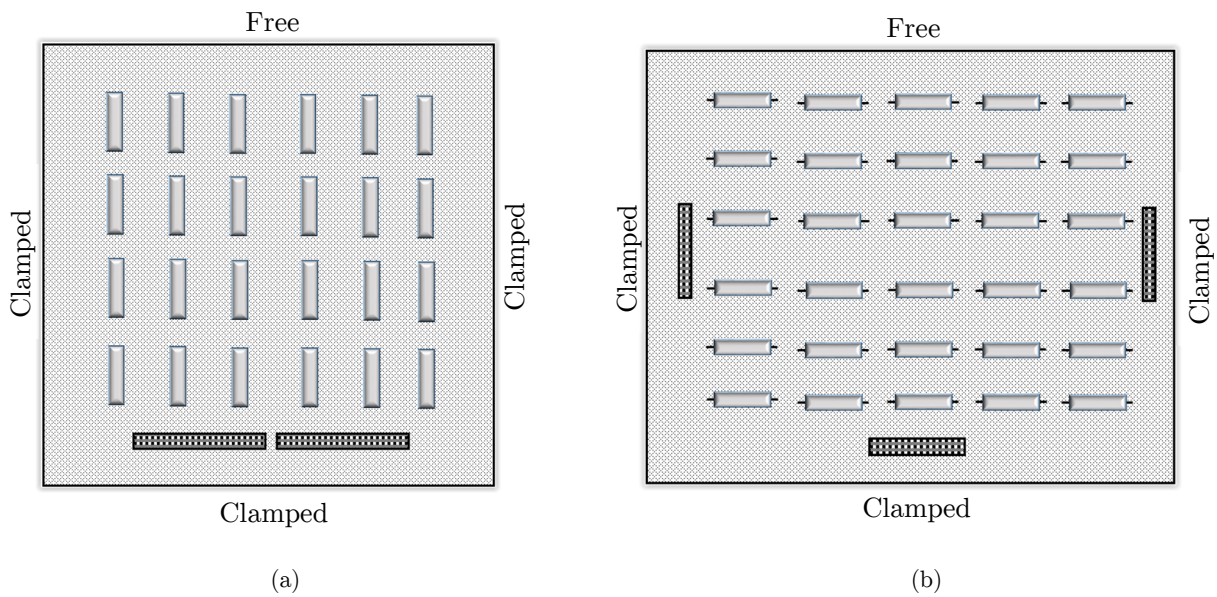

Figure 8: Test setup (Genç 2006): a) PDIP; b) Tantalum Capacitor.

The geometric parameters of the PDIP's leads of CDA 194 (copper) are: b_1 = 1.715 mm; b_2 = 0.551 mm; l_1 = 1.65 mm; l_2 = 0.5 mm and t = 0.304 mm. The model of the capacitor's leads of nickel has: a = 3.5 mm, b = 4.51 mm and diameter of 0.64 mm.

Both tests were executed through vibration steps of 60 minutes each in the frequency range of 20 to 2000 Hz with constant PSD. Step 1 level is 2.02×10^{-3} g^2Hz^{-1} and step 14 level is 6.694×10^{-3}

g^2Hz^{-1}. The PSD ratio between steps is close to 1.56. Genç (2006) has not achieved failures for the PDIDs. For these components, the test started at step 3 and lasted until 2.5 minutes of step 14, when the shaker aborted. Then, any result higher than 662.5 minutes for the PDIPs lifetime is in agreement with the experimental tests. The capacitors test started at step 1 and failed mainly in steps 3 and 4.

The comparisons between experimental and analytical times to failure are described in Tables 10 and 11. The results presented by Genç (2006) were not discriminated by EC positions on the board. Therefore, it was only possible to compare the ranges of times to failure.

The present analyses performed step 14 without a time constraint, so it could surpass 60 minutes. The PDIPs calculated natural frequency of 55730 Hz is much higher than the vibrated band of 20 to 2000Hz. Thus, the acceleration stretch almost did not contribute in fatigue. The capacitors calculated natural frequency of 990 Hz is inside the vibrated band of 20 to 2000Hz. Therefore, the acceleration stretch (Eq. 13) is the most damaging contributor, and the middle region of the PCB is the most critical one for the capacitors. The present results are of the same magnitude order of the experimental ones.

Steinberg's method showed to be conservative for the PDIDs, and optimistic for the capacitors. In the case of the capacitors, Steinberg's method failed in describing the time to failure by not considering the EC natural frequency. This is evident when comparing the similarity between the acceleration off model to Steinberg's results.

Model	$x=\overline{a}$ /2; $y=\overline{b}$ /2 (Fig. 3)	$x=\overline{a}$ /10; $y=\overline{b}$ /10 (Fig. 3)	$x=\overline{a}$ /4; $y=\overline{b}$ /4 (Fig. 3)	Fail Point (Fig. 1)
Complete / 9 modes	>step 14 (8.43×10^2)	step 14 (6.64×10^2)	step 14 (7.05×10^2)	no fail
Acceleration off	>step 14 (8.70×10^2)	step 14 (6.64×10^2)	step 14 (7.06×10^2)	no fail
Moment off	>step 14 (8.60×10^2)	step 14 (6.64×10^2)	step 14 (7.08×10^2)	no fail
Complete / 1 mode	>step 14 (9.65×10^2)	step 14 (6.67×10^2)	step 14 (7.12×10^2)	no fail
Steinberg (2000)	step 10 (5.43×10^2)	step 13 (7.27×10^2)	step 11 (6.31×10^2)	not available
Genç (2006)	step 3 up to 2.5 min. of step 14 with no failure total time: 6.62×10^2			no fail

Table 10: Failure step (minutes to failure) for PDIP.

Model	$x=\overline{a}$ /2; $y=\overline{b}$ /2 (Fig. 3)	$x=\overline{a}$ /10; $y=\overline{b}$ /10 (Fig. 3)	$x=\overline{a}$ /4; $y=\overline{b}$ /4 (Fig. 3)	Fail Point (Fig. 1)
Complete / 9 modes	step 3 (1.52×10^2)	step 6 (3.07×10^2)	step 3 (1.59×10^2)	*a*
Acceleration off	step 9 (5.22×10^2)	>14 step	step 12 (6.62×10^2)	*a*
Moment off	step 2 (1.01×10^2)	step 5 (2.53×10^2)	step >14 (9.90×10^2)	*a*
Complete / 1 mode	step 4 (2.07×10^2)	step 4 (1.89×10^2)	step 7 (4.06×10^2)	*a*
Steinberg (2000)	step 11 (5.17×10^2)	step 13 (7.20×10^2)	step 11 (6.12×10^2)	not available
Genç (2006)	first fail: between step 3 and 4 (1.52×10^2 and 2.04×10^2) eleventh fail: step 6 (3.50×10^2)			*a*

Table 11: Failure step (minutes to failure) for tantalum capacitor.

4 CONCLUSIONS

A novel analytical model is presented to predict the useful life of electronic components under random vibration. The complete/ 9 modes model presented the closest approximation to the experimental results. As this is the most complete model, and seemed to be always more conservative than the others, this is the recommended configuration. The acceleration off model excludes the acceleration stretch term ($\delta_{ca,mn}$). Its fatigue lives estimation varied from 0%, for stiff lead attachments, to 316% higher than Complete/9 modes model, for the most flexible one (Tantalum). The moment off configuration proved the importance of the PCB bending effects, since it presented in average life estimation values 35% higher than the recommended model, and the increase in fatigue life estimation varied between 0% and 522%. The complete/ 1 mode model results depend on the test frequency range: for a large range, this model is 4% to 14% higher in life to failure estimation than the recommended model, with a maximum of 155% for the Tantalum capacitor.

The lifetime predictions for the full present model are of the same magnitude order of the experimental findings. The obtained results are more accurate than the Steinberg's method and could predict reasonable results for all electronic components studied. Steinberg's method failed mainly in components where EC's natural frequency is relatively low (Tantalum Capacitors). The proposed method calculates the distributed stress along the leads, what allows a workaround in case of fatigue problems.

The objective of creating an accurate model with low computational cost has been achieved. The practical applications show that the model is suitable for design of aerospace vehicle electronic embedded systems, or any other vehicle exposed to dynamic loads.

References

Amy, R. A., Aglietti, G. S., Richardson G., (2010). Accuracy of simplified printed circuit board finite element models, Elsevier Microelectronics Reliability 50: 86-97.

Amy, A., Aglietti, G. S., Richardson, G., (2010). Board-level vibration failure criteria for printed circuit assemblies: An experimental approach, IEEE Transactions on electronics packaging manufacturing 33, No. 4: 303-311.

Amy, A., Aglietti, G. S., Richardson, G., (2009). Reliability analysis of electronic equipment subjected to shock and vibration – A review, Shock and Vibration 16: 45-59.

Amy, R. A., Aglietti, G. S., Richardson, G., (2006). Simplified modeling of printed circuit boards for spacecraft applications, 57th International Astronautical Congress.

ASTM (American Society for testing and materials) (2011). E1049-85: Standard practices for cycle counting in fatigue analysis.

Basaran, C., Jiang, J., (2002). Measuring intrinsic elastic modulus of Pb/Sn solder alloys, Mechanics of Materials 34: 349-362.

Blevins, R. D., (2001). Formulas for natural frequency and mode shape, Krieger Publishing Company (New York).

Cifuentes, A. O., (1994). Estimating the dynamic behavior of printed circuit boards, IEEE Transactions on components, packaging, and manufacturing technology-part B: Advanced packaging 17: 69-75.

Dirlik, T., (1985). Application of computers in fatigue analysis, Ph.D. Thesis, University of Warwick, Coventry, UK.

Esser, B., Huston, D., (2003). Active mass damping of electronic circuit boards, Elsevier Journal of Sound and Vibration.

Fairchild Semiconductor (2001). 68-Lead plastic leaded chip carrier (PLCC): package dimensions.

Genç, C., (2006). Mechanical fatigue and life estimation analysis of printed circuit board components, Thesis of Science Master Degree, Middle East Technical University, Beirut, Lebanon.

Grieu, M., Massiot, G., Maire, O., Chaillot, A., Bienvenu, C. M. Y., Renard, J., (2008). Durability Modeling of a BGA Component under Random Vibration, Mechanical and Multiphysics Simulation and Experiments in Micro-Electronics and Micro-Systems, IEEE 9th. Int. Conf. on Thermal, EuroSimE.

Lalanne, C., (2002). Mechanical vibration & shock: Random vibration, Hermes Penton Ltd (London).

Liguore, S., Followell, D., (1995). Vibration fatigue of surface mount technology (SMT) solder joints, IEEE Proceedings Annual Reliability and Maintainability Symposium.

Mrnik, M., Slavic, J., Boltezar, M., (2012). Frequency-domain methods for a vibration-fatigue-life estimation – Application to real data, International Journal of Fatigue 47: 8-17.

Sayles, A. A., Stoumbos, T., (2015). Evaluating the dynamic behavior and analytically predicted displacements of printed circuit boards (PCBs) using the "smeared-mass" & fine mesh approach, 56th AIAA/ASCE/AHS/ASC Structures, Structural Dynamics, and Materials Conference.

Singal, R. K., Gorman, D. J., Forgues, S. A., (1992). A comprehensive analytical solution for free vibration of rectangular plates with classical edge conditions: Experimental Verification, Experimental Mechanics: 21-23.

Silva, G. H. C., Gonçalves, P. J. P., (2013). A model for computing vibration induced stresses of electronic components in a general flexible mounting, Elsevier Journal of Sound and Vibration 332: 5192-5206.

Steinberg, D. S., (2000). Vibration analysis for electronic equipment, John Wiley Sons (New York).

Sumitomo Bakelite (2000). Environmentally friendly epoxy molding compound for semiconductor: Sumikon EME-G series.

Texas Instruments (2001). SMJ320C25, SMJ320C25-50: digital signal processor.

Veprik, A. M., Barbitsky, V. I., (2000). Vibration protection of sensitive electronic equipment from harsh harmonic vibration, Elsevier Journal of Sound and Vibration 238: 19-30.

Veprik, A. M., (2003). Vibration protection of critical components of electronic equipment in harsh environmental conditions, Elsevier Journal of Sound and Vibration 259: 161-175.

Wong, T. E., Reed, B. A., Cohen, H. M., Chu, D. W., (2000). Development of BGA solder joint vibration fatigue life prediction model, IEEE.

Wu, M. L., (2009). Vibration-induced fatigue life estimation of ball grid array packaging, Journal Micromechanics and Microengineering 19.

Yang, Q. J., Wang, Z. P., Lim, G. H., Pang, J. H. L., Yap, F. F., Lin, R. M., (2002). Reliability of PBGA assemblies under out-of-plane, IEEE Transactions on components and packaging technologies 25, No. 2: 293-300.

Yang, Q. J., Pang, H. L. J., Wang, Z. P., Lim, G. H., Yap, F. F., Lin, R. M., (2000). Vibration reliability characterization of PBGA assemblies, Pergamon Microelectronics Reliability 40: 1097-1107.

Yu, D., Al-Yafawi, A., Nguyen, T. T., Park, S., Chung, S., (2011). High-cycle fatigue life prediction for Pb-free BGA under random vibration loading, Elsevier Microelectronics Reliability 51: 649-656.

APPENDIX A: ELECTRONIC COMPONENT KINEMATICS

The electronic component movement due to PCB displacements can be expressed as

$$Z_{c,mn}\left(x,y\right) = Z_0 + \left(x-\overline{e}\right)\theta_c + \left(y-\overline{f}\right)\phi_c \tag{A.1}$$

where the variables Z_0, θ_c and ϕ_c can be evaluated according to the following equations:

$$Z_0 = \frac{4\overline{a}\overline{b}}{\pi^2 mn\overline{c}\overline{d}} \frac{2B_{mn}\left(W\right)}{\sqrt{\rho\overline{a}\overline{b}}} sen\left(\frac{n\pi\overline{f}}{\overline{b}}\right) sen\left(\frac{n\pi\overline{d}}{2\overline{b}}\right) sen\left(\frac{m\pi\overline{e}}{\overline{a}}\right) sen\left(\frac{m\pi\overline{c}}{2\overline{a}}\right) \tag{A.2}$$

$$\begin{aligned}\theta_c = \frac{12}{\overline{d}\overline{c}^3} \frac{2\overline{b}}{\pi mn} \frac{2B_{mn}\left(W\right)}{\sqrt{\rho\overline{a}\overline{b}}} sen\left(\frac{n\pi\overline{f}}{\overline{b}}\right) sen\left(\frac{n\pi\overline{d}}{2\overline{b}}\right) \left\{\frac{2\overline{a}^2}{\pi^2 m} sen\left(\frac{m\pi\overline{c}}{2\overline{a}}\right) sen\left(\frac{m\pi\overline{e}}{\overline{a}}\right)\right. \\ \left. - \frac{\overline{a}}{\pi}\left[\overline{c}\cos\left(\frac{m\pi\overline{e}}{\overline{a}}\right)\cos\left(\frac{m\pi\overline{c}}{2\overline{a}}\right) - 2\overline{e} sen\left(\frac{m\pi\overline{e}}{\overline{a}}\right) sen\left(\frac{m\pi\overline{c}}{2\overline{a}}\right)\right] - \frac{2\overline{a}\overline{e}}{\pi} sen\left(\frac{m\pi\overline{e}}{\overline{a}}\right) sen\left(\frac{m\pi\overline{c}}{2\overline{a}}\right)\right\}\end{aligned} \tag{A.3}$$

$$\begin{aligned}\phi_c = \frac{12}{\overline{c}\overline{d}^3} \frac{2\overline{a}}{\pi mn} \frac{2B_{mn}\left(W\right)}{\sqrt{\rho\overline{a}\overline{b}}} sen\left(\frac{n\pi\overline{e}}{\overline{a}}\right) sen\left(\frac{n\pi\overline{c}}{2\overline{a}}\right) \left\{\frac{2\overline{b}^2}{\pi^2 m} sen\left(\frac{m\pi\overline{d}}{2\overline{b}}\right) sen\left(\frac{m\pi\overline{f}}{\overline{b}}\right)\right. \\ \left. - \frac{\overline{b}}{\pi}\left[\overline{d}\cos\left(\frac{m\pi\overline{f}}{\overline{b}}\right)\cos\left(\frac{m\pi\overline{d}}{2\overline{b}}\right) - 2\overline{f} sen\left(\frac{m\pi\overline{f}}{\overline{b}}\right) sen\left(\frac{m\overline{d}}{2\overline{b}}\right)\right] - \frac{2\overline{b}\overline{f}}{\pi} sen\left(\frac{m\pi\overline{f}}{\overline{b}}\right) sen\left(\frac{m\pi\overline{d}}{2\overline{b}}\right)\right\}\end{aligned} \tag{A.4}$$

The PCB curvature and the lead total rotations are calculated by:

- PCB rotation around y axis

$$\theta_{PCB}\left(x,y,W\right) = \frac{\partial Z_{mn}\left(x,y,W\right)}{\partial x} = \frac{2m\pi B_{mn}\left(W\right)}{\overline{a}\sqrt{\rho\overline{a}\overline{b}}} \cos\left(\frac{m\pi x}{\overline{a}}\right) \sin\left(\frac{n\pi y}{\overline{b}}\right) \tag{A.5}$$

- PCB rotation around x axis

$$\phi_{PCB}\left(x,y,W\right) = \frac{\partial Z_{mn}\left(x,y,W\right)}{\partial y} = \frac{2n\pi B_{mn}\left(W\right)}{b\sqrt{\rho\overline{a}\overline{b}}} \sin\left(\frac{m\pi x}{\overline{a}}\right) \cos\left(\frac{n\pi y}{\overline{b}}\right) \tag{A.6}$$

- Lead lateral 1 (bending) rotation due to the P force in the extremity 2 (longitudinal stretch)

$$\theta_2 = P\left(\frac{c^2}{2EI_{z'2}} + \frac{b_2 c}{EI_{z'2}} + \frac{b_1 c}{EI_{z'1}} + \frac{\left(a^2 + 2ac\right)}{2EI_{z'1}} - \frac{\left(a+c\right)d}{EI_{z'1}}\right) \tag{A.7}$$

- Lead lateral 1 (bending) rotation around y axis

$$\theta_{lead,lat1}\left(x,y,W\right) = \left[\theta_{PCB}\left(x,y,W\right) - \theta_c\left(W\right) - \theta_2\left(x,y,W\right)\right] fat_{cm1}\left(x,y\right) \tag{A.8}$$

- Lead lateral 2 (torsion) rotation around y axis

$$\theta_{lead,lat2}\left(x,y,W\right) = \left[\theta_{PCB}\left(x,y,W\right) - \theta_c\left(W\right)\right] fat_{cm2}\left(x,y\right) \tag{A.9}$$

- Lead lateral 1 (bending) rotation around x axis

$$\phi_{lead,lat1}\left(x,y,W\right) = \left[\phi_{PCB}\left(x,y,W\right) - \phi_c\left(W\right) - \theta_2\left(x,y,W\right)\right] fat_{cm1}\left(x,y\right) \tag{A.10}$$

- Lead lateral 2 (torsion) rotation around x axis

$$\phi_{lead,lat2}\left(x,y,W\right)=\left[\phi_{PCB}\left(x,y,W\right)-\phi_{c}\left(W\right)\right]fat_{cm2}\left(x,y\right) \tag{A.11}$$

APPENDIX B: SUMMARY OF DIRLIK FATIGUE DAMAGE METHOD

The Dirlik fatigue damage method variables are resumed below (Mrnik 2012):

$$m_{i}=\frac{1}{2\pi}\int_{0}^{+\infty}W^{i}\sigma_{VM}\left(W\right)dW \tag{B.1}$$

$$\alpha_{2}=\frac{m_{2}}{\sqrt{m_{0}m_{4}}} \tag{B.2}$$

$$x_{m}=\frac{m_{1}}{m_{0}}\left(\frac{m_{2}}{m_{4}}\right)^{1/2} \tag{B.3}$$

$$G_{1}=\frac{2\left(x_{m}-\alpha_{2}^{2}\right)}{1+\alpha_{2}^{2}} \tag{B.4}$$

$$R=\frac{\alpha_{2}-x_{m}-G_{1}^{2}}{1-\alpha_{2}-G_{1}+G_{1}^{2}} \tag{B.5}$$

$$G_{2}=\frac{1-\alpha_{2}+G_{1}+G_{1}^{2}}{1+R} \tag{B.6}$$

$$G_{3}=1-G_{1}-G_{2} \tag{B.7}$$

$$Q=\frac{1.25\left(\alpha_{2}-G_{3}-G_{2}R\right)}{G_{1}} \tag{B.8}$$

APPENDIX C: SUMMARY OF PCB AND EC PROPERTIES

The PCB and EC properties used on the calculations are presented on tables C.1 and C.2. The properties were obtained preferably in the reference paper (Liguore and Followell (1995) / YU et al (2011) / Genç (2006)). Otherwise the data was taken from components datasheet or from Steinberg (2000).

PCB properties	$\overline{a}$ (mm)	$\overline{b}$ (mm)	Material	t_{PCB} (mm)	E_{PCB} (Mpa)	ν_{PCB}
PLCC / LCCC	304.8[1]	152.4[1]	E-Glass[1]	1.45[1]	80000	0.3
PBGA	85[2]	45[2]	FR4[2]	0.6[2]	25000[2]	0.28[2]
PDIP/ Capacitor	318[3]	233[3]	not available	2.5*	17000[3]	0.3[3]

(References: 1 - Liguore and Followell (1995) ; 2 - YU et al (2011) ; 3 - Genç (2006))

Table C.1: PCB properties.

EC properties	mass (g)	lead material	E_{lead} (Mpa)	body material	E_{body} (Mpa)	a (mm)	b_1 (mm)	b_2 (mm)	c (mm)
PLCC	10*	Copper[1]	128000	Plastic[1]	26000[5]	0.08[7]	1.53[7]	1.53[7]	0[7]
LCCC 32	10*	Pb solder[1]	44000[6]	Ceramic[1]	275700[4]	0[8]	0.305[8]	0.305[8]	0[8]
LCCC 68	10*	Pb solder[1]	44000[6]	Ceramic[1]	275700[4]	0[8]	0.425[8]	0.425[8]	0[8]
LCCC 84	10*	Pb solder[1]	44000[6]	Ceramic[1]	275700[4]	0[8]	0.425[8]	0.425[8]	0[8]
PBGA	0.21[2]	SAC 305[2]	51000[2]	Plastic[2]	20900[2]	0[2]	0.2[2]	0.01[2]	0[2]
PBGA	0.21[2]	SAC 405[2]	51000[2]	Plastic[2]	20900[2]	0[2]	0.2[2]	0.01[2]	0[2]
PDIP	1.08[3]	CDA194[3]	121000[3]	Plastic[3]	14500[3]	0.457[3]	1.715[3]	0.551[3]	0[3]
Cap. Tant.	6.04[3]	Nickel[3]	207000[3]	-	186000[3]	3.5[3]	4.5[3]	0[3]	0[3]

(References: 1 - Liguore and Followell (1995) ; 2 - YU et al (2011) ; 3 - Genç (2006) ; 4 - Steinberg (2000) ; 5 - Sumitomo Bakelite (2000); 6 – Basaran and Jiang (2002) ; 7 – Fairchild Semiconductor (2001) ; 8 – Texas Instruments (2001))

Table C.2: EC properties.

EC prop.	d (mm)	l_1 (mm)	l_2 (mm)	t_{leads} (mm)	$\overline{c}$ (mm)	$\overline{d}$ (mm)	t_c (mm)	C_b (MPa)	b_b
PLCC	0[7]	0.735[7]	0.43[7]	0.25[7]	25[7]	25[7]	4.125[7]	1.57e19[4]	6.5[4]
LCCC 32	0[8]	1.27[8]	1.27[8]	cylinder	13[8]	13[8]	1.83[8]	4.032e9[4]	4[4]
LCCC 68	0[8]	1.27[8]	1.27[8]	cylinder	24[8]	24[8]	2.55[8]	4.032e9[4]	4[4]
LCCC 84	0[8]	1.27[8]	1.27[8]	cylinder	29[8]	29[8]	2.55[8]	4.032e9[4]	4[4]
PBGA	0[2]	0.266[2]	0.22[2]	cylinder[2]	10.5[2]	10.5[2]	1[2]	4.454e12[2]	7[2]
PBGA	0[2]	0.266[2]	0.22[2]	cylinder[2]	10.5[2]	10.5[2]	1[2]	2.534e10[2]	4.75[2]
PDIP	0[3]	1.65[3]	1.65[3]	0.3045[3]	19[3]	9[3]	3.43[3]	4.345e20[4]	6.5[4]
Cap. Tant.	0[3]	0.64[3]	0.64[3]	cylinder[3]	9[3]	19[3]	9[3]	9.051e17[4]	6.5[4]

(References: 1 - Liguore and Followell (1995) ; 2 - YU et al (2011) ; 3 - Genç (2006) ; 4 - Steinberg (2000) ; 5 – Sumitomo Bakelite (2000); 6 – Basaran and Jiang (2002) ; 7 – Fairchild Semiconductor (2001) ; 8 – Texas Instruments (2001))

Table C.2: EC properties (continuation).

* Property not available. Value calculated in order to fit the PCB first natural frequency.